

## Meteorological Processes Affecting the Evolution of a Wintertime Cold Air Pool in the Columbia Basin

SHIYUAN ZHONG, C. DAVID WHITEMAN, XINDI BIAN, WILLIAM J. SHAW, AND JOHN M. HUBBE

*Pacific Northwest National Laboratory, Richland, Washington*

(Manuscript received 26 September 2000, in final form 28 February 2001)

### ABSTRACT

Meteorological mechanisms affecting the evolution of a persistent wintertime cold air pool that began on 2 January and ended on 7 January 1999 in the Columbia basin of eastern Washington were investigated using a mesoscale numerical model together with limited observations. The mechanisms include surface radiative cooling and heating, large-scale subsidence, temperature advection, downslope warming in the lee of a major mountain barrier, and low-level cloudiness.

The cold pool began when cold air accumulated over the basin floor on a clear night and was maintained by a strong capping inversion resulting from a rapid increase of air temperatures above the cold pool. This increase of temperatures aloft was produced primarily by downslope warming associated with strong westerly winds descending the lee slopes of the north-south-oriented Cascade Mountains that form the western boundary of the Columbia basin. While the inversion cap at the top of the cold pool descended with time as the westerly flow intensified, the air temperature inside the cold pool exhibited little variation because of the fog and stratus accompanying the cold pool. Although the low-level clouds reduced the diurnal temperature oscillations inside the pool, their existence was not critical to maintaining the cold pool because surface radiative heating on a midwinter day was insufficient to completely destroy the temperature deficit in the persistent inversion. The presence of low-level clouds becomes much more critical for the maintenance of persistent cold pools in the spring and, perhaps, the fall seasons when insolation is much stronger than in midwinter. The cold pool was destroyed by cold air advection aloft, which weakened and eventually removed the strong inversion cap, and by an unstable boundary layer that grew upward from the heated ground after the dissipation of low-level clouds. Finally, erosion of the cold pool from above by turbulent mixing produced by vertical wind shear at the interface between quiescent air within the pool and stronger winds aloft was found to be insignificant for this case.

### 1. Introduction

Persistent cold air pools, that is, cold pools lasting longer than one diurnal cycle, are a prominent feature of wintertime meteorology for many basin areas of the world. For example, in the Columbia basin of eastern Washington persistent cold pools occur, on average, three to four times each during December and January (Whiteman et al. 2001). Midwinter multiday cold pools are also known to form frequently over the Colorado plateau basin (Whiteman et al. 1999) and over the intermountain basin of the western United States (Wolyn and McKee 1989). Persistent cold pools also form in the basins of Slovenia and Croatia (Petkovsek 1992; Vrhovc 1991) in wintertime. Persistent cold pools can produce prolonged periods of relatively cold, dreary weather. Because of their stable stratification and relatively weak winds, they can trap air pollutants released inside the pool for many days, allowing pollutant concentrations to build up to high levels and producing

severe air quality problems. Forecasting the buildup and removal of persistent wintertime cold pools is hampered by our current lack of understanding of the mechanisms involved and is considered one of the most challenging forecast problems in basin and valley areas of the United States (Smith et al. 1997).

Despite their large impact on weather and air pollution in basins and valleys, persistent cold pools have received little research attention. The few existing studies in the literature have been carried out mainly by Slovenian scientists. Petkovsek (1992) modeled cold pool dissipation due to turbulent erosion at the cold pool top by solving a simplified turbulent kinetic energy equation. His results indicated that dissipation of a cold pool from above can be initiated by a  $9 \text{ m s}^{-1}$  wind speed just above the cold pool, and that an increase in wind speeds above the pool with time is necessary for the continuation of the dissipation process. Using a two-dimensional numerical model, Vrhovc and Hrabar (1996) examined the role of diabatic heating, cold air advection, and turbulent erosion on cold pool destruction. For an idealized basin cross section, they found that in wintertime cold air advection and increasing

---

*Corresponding author address:* Shiyuan Zhong, Pacific Northwest National Laboratory, P.O. Box 999, K9-30, Richland, WA 99352.  
E-mail: shiyuan.zhong@pnl.gov

wind speed aloft can cause sufficient mixing to dissipate deep cold pools, while surface thermal forcing is often insufficient, especially when the ground is covered by snow. Vrhovec (1991) applied a three-dimensional mesoscale model to a case study of cold pool formation in the Slovenj Gradec basin, an alpine basin in northern Slovenia. He found that cold pool formation could completely decouple the winds at lower and higher altitudes, resulting in an abrupt change in wind speed and direction at the top of the pool. These Slovenian studies are the only ones that have focused on cold pool formation and destruction, but no observational data were available to support their modeling results.

A numerical study carried out by Lee et al. (1989) examined the influence of a cold pool downstream of a bell-shaped mountain on the generation of downslope windstorms. The simulations showed that when a cold pool is present downstream of a mountain, the development of large-amplitude mountain waves is inhibited and the associated downslope winds can be prevented from penetrating the cold pool to reach the surface and flush out the stable cold air. Shear-induced turbulent mixing at the top of the cold air was found to have little effect on flushing and, in the absence of significant surface heating, a favorable large-scale surface pressure gradient force must be involved to remove the cold pool before the downslope winds can actually reach the surface. As was the case for the Slovenian studies mentioned above, its idealized terrain configuration and lack of support from observations limited this modeling study.

Observations of cold pools have been limited because of the difficulty and expense of making upper-air soundings at a frequency and vertical resolution that can capture the vertical structure and evolution of cold pools. Wolyn and McKee (1989), Savoie and McKee (1995), and Mayr and McKee (1995) carried out climatological studies of persistent stagnation episodes in the intermountain basin of the western United States. They found that surface-based stable layers or cold pools in the intermountain basin are sometimes produced by flow blocking upstream of the Rocky Mountains and that these cold pools can be destroyed rather abruptly by passing short-wave troughs. Whiteman et al. (1999) investigated cold pools that form over the Colorado plateau basin. They found that persistent cold pools may develop there following arctic air intrusions or following clear nights when cold air drains into the basin from surrounding mountains. Cold pools strengthen and weaken as weather systems pass through the southwestern United States with their associated warm and cold air advection above the pool. Standard twice-daily rawinsonde soundings provided insufficient temporal information to allow detailed investigations of some cold pool evolution processes.

Recent advances in remote sensing instruments and computational power along with improvements in model parameterizations and numerical algorithms have made

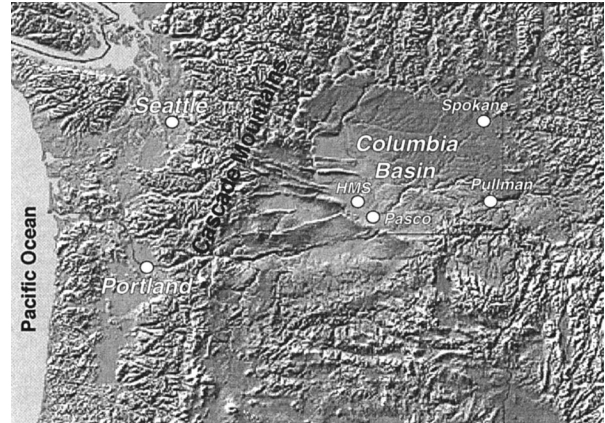


FIG. 1. The terrain of the Columbia basin and the locations of HMS and selected National Weather Service surface weather stations in eastern WA.

detailed studies of cold pools possible so that an in-depth understanding of the processes affecting cold pool formation and destruction can be achieved. During the period from 1 November 1998 to 1 March 1999, measurements using in situ and remote sensing instruments were made in south-central Washington for studies of cold pool evolution in the lower Columbia basin. Whiteman et al. (2001) summarized the characteristics of the persistent cold pools that occurred during the 4-month observational period and presented a climatology of cold pools in the lower Columbia basin from surface temperature data collected over a 10-yr period. The current paper describes a detailed numerical study, using a high-resolution mesoscale numerical model, of the longest cold pool episode observed during the winter of 1998–99. The focus of this modeling study is to evaluate the relative importance of different physical mechanisms in the formation, maintenance, and destruction of this persistent wintertime cold pool. Section 2 gives a brief description of the topography of the Columbia basin, the measurements, and the particular episode. Section 3 describes the mesoscale model and the specific model configuration. Results and discussions are presented in section 4. This is followed by the summary and conclusions in section 5.

## 2. Observations

The Columbia basin (Fig. 1) occupies most of eastern Washington and parts of eastern Oregon. The basin is bounded by the Cascade Mountains to the west, the Blue Mountains to the south and southeast, and the Rocky Mountains to the north and east. The Columbia basin is intermediate in scale between the aforementioned small Slovenian basins and the larger Colorado plateau and intermountain basins. Because of the rain shadow effect of the Cascade Mountains, the Columbia basin is semiarid. Within the Columbia basin, there are several subbasins located along the path of the Columbia River.

Measurements were made in south-central Washington in the Pasco subbasin, the lowest subbasin of the Columbia basin, which has elevations generally below 200 m above mean sea level (MSL). The evolution of the vertical structure of the cold pool in this subbasin was measured with an instrumented tower and a 915-MHz radar wind profiler/radio acoustic sounding system (RASS) at the Hanford Meteorological Station (HMS, elevation 213 m MSL; see Fig. 1). The tower provided 15-min average values of temperature and humidity at eight levels (1, 9, 15, 30, 61, 76, 91, and 119 m) and wind speed and direction at four levels (9, 15, 61, and 119 m). Wind and temperature profiles from the profiler/RASS were reported at 100-m vertical height intervals from about 100 m above ground level (AGL) up to 2500 and 1500 m AGL, respectively. The data were reported every half hour with an averaging time of 20 min for wind and 10 min for temperature. Vertical temperature structure data were also obtained from a line of commercial temperature dataloggers installed at 100-m-altitude intervals along the slope of Rattlesnake Mountain, a mountain that forms part of the southwestern boundary of the Pasco subbasin. In addition, there were over 30 surface meteorological stations within the Pasco subbasin as well as one station on top of Rattlesnake Mountain at 1074 m MSL. A detailed description of the various instruments, their accuracy, and measurement frequencies was given by Whiteman et al. (2001).

Although cold pool episodes occur, on average, 3–4 times per month in December and January in the Pasco subbasin (Whiteman et al. 2001), the winter of 1998–99 was atypical in having fewer and shorter cold pools than average. The longest cold pool, which occurred between 2 and 7 January, is the focus of the present numerical study.

The synoptic conditions accompanying this cold pool episode are illustrated in Fig. 2, which shows the evolution of 850-hPa geopotential height, temperature, and wind fields at 24-h intervals beginning at 1600 Pacific Standard Time (PST) on 2 January. The 850-hPa pressure level is near or above the ridgelines of the mountains surrounding the Columbia basin and, therefore, provides information on winds and temperature advection above the cold pool. At the beginning of this 5-day period, a high pressure center was just offshore of the Washington coast. Winds were light over the region and temperatures were 4° to 5°C over western Washington and –5° to 0°C over the eastern part of the state. In the next 24 h, this high pressure weakened somewhat and moved slightly inland while another high pressure system developed at the Oregon–Nevada border. Winds were still light, but temperatures increased by several degrees Celsius throughout Washington due to subsidence associated with the high pressure center. On 4 January, the high pressure system over the Washington coast gave way to a broad ridge, and the increased pressure gradient produced westerly winds over the state. Temperatures over eastern Washington increased by 1°–

2°C, while temperatures on the west side actually dropped slightly during this time period. As the westerly winds increased from 4 to 5 January, temperatures remained almost unchanged over western Washington, but increased rapidly on the eastern side. The rapid temperature rise over eastern Washington could be attributed to two factors: large-scale warm air advection and/or mesoscale downslope warming as the westerly winds descended the lee slopes of the north–south-oriented Cascade Mountains. The fact that winds were directly from the west over both sides of the Cascades while temperatures west of the Cascades remained essentially unchanged points to the downslope warming as the most likely cause for the temperature rise east of the Cascades including the Columbia basin. The westerly winds that prevailed on 4 and 5 January shifted to northwesterly on 6 January when a ridge developed upstream of Washington and Oregon as a high pressure system strengthened off the California coast. The strong northwesterly winds brought cold air from the Gulf of Alaska to the Pacific Northwest, producing a rapid decrease in temperatures over the region. The cooling continued through 7 January as the northwesterly winds prevailed.

The evolution of the temperature structure in the lowest 1200 m in the Pasco subbasin was measured by the RASS and temperature sensors on the 122-m tower at HMS and is shown in Fig. 3a. The rest of the plots in Fig. 3 (3b–3f) are results from different numerical simulations to be discussed later in section 4. The 15-min tower temperature data were averaged to obtain half-hourly values comparable with the RASS records. The corresponding evolution of horizontal winds measured by the radar wind profiler at HMS is shown in Fig. 4a. Figure 3a shows that cold air began to accumulate over the basin floor during the clear night on 2 January. As the temperature dropped, fog started to form on the morning of 3 January and then lifted to form low stratus. The fog and low stratus persisted over the basin during the next few days and, as a result, temperatures at the lowest altitudes of the basin remained near or below freezing with little diurnal variation. Winds on 2 and 3 January were near calm, reflecting the control of the high pressure center over the region as shown in Fig. 2, and temperatures aloft increased gradually due to subsidence. Beginning on the late morning of 4 January and continuing through 5 January, temperatures above the basin increased rapidly as moderate to strong westerly winds prevailed over the area. As indicated earlier, this rapid increase in temperatures aloft was likely to be caused by downslope warming when the westerly flow descended the lee slopes of the Cascade Mountains. The rapid warming produced a strong inversion cap on top of the cold pool that descended with time as the downslope flow intensified. This strong capping inversion trapped the cold air within the basin until the afternoon of 6 January when the inversion was weakened and eventually removed by cold air advection associated with the shift in wind direction aloft from westerly to

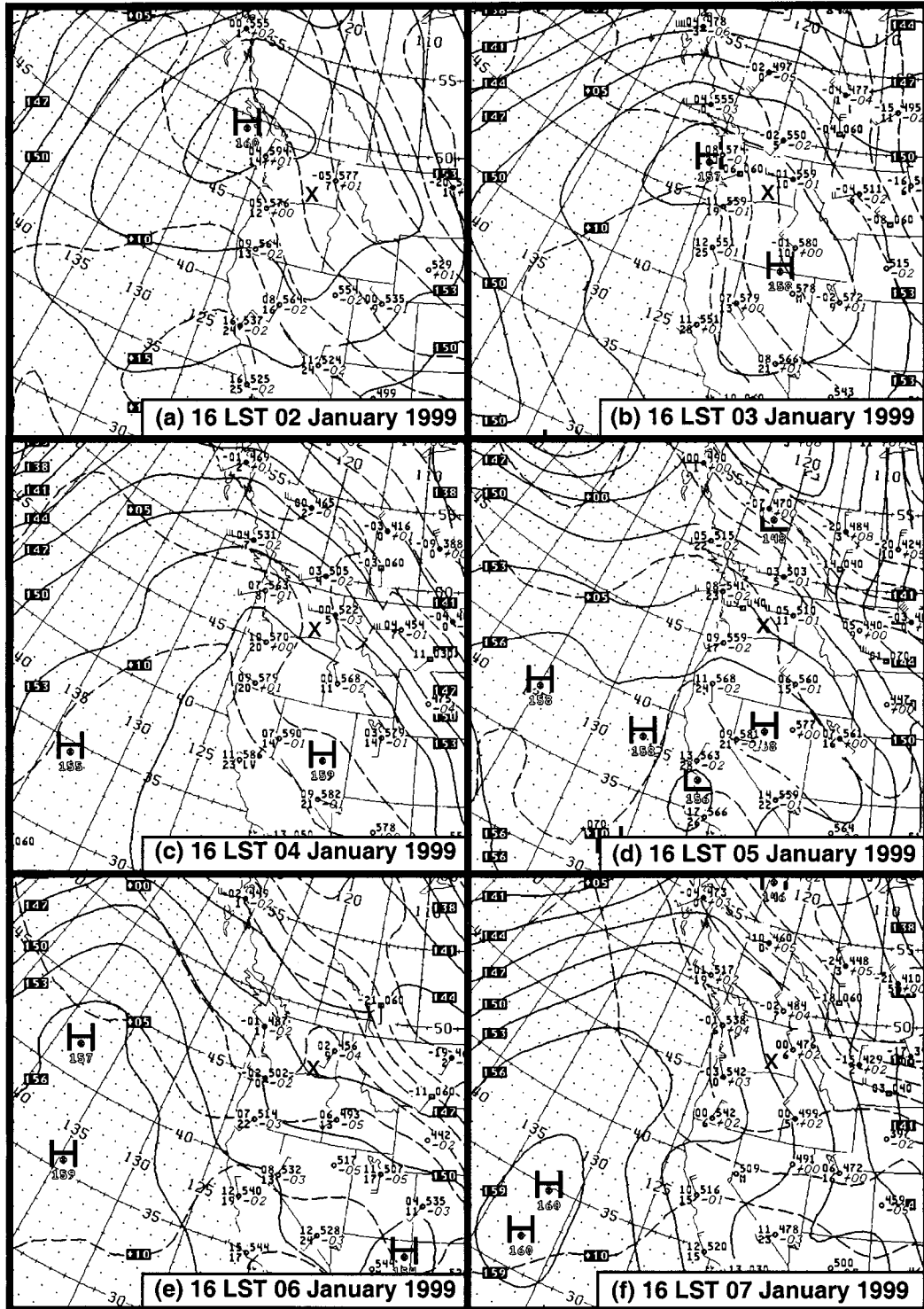


FIG. 2. The 850-hPa upper air analyses at 24-h intervals starting at 1600 PST 2 Jan and ending at 1600 PST 7 Jan 1999. Solid lines are geopotential height contours in dm; dashed lines are temperature contours in °C. An X marks the location of HMS.

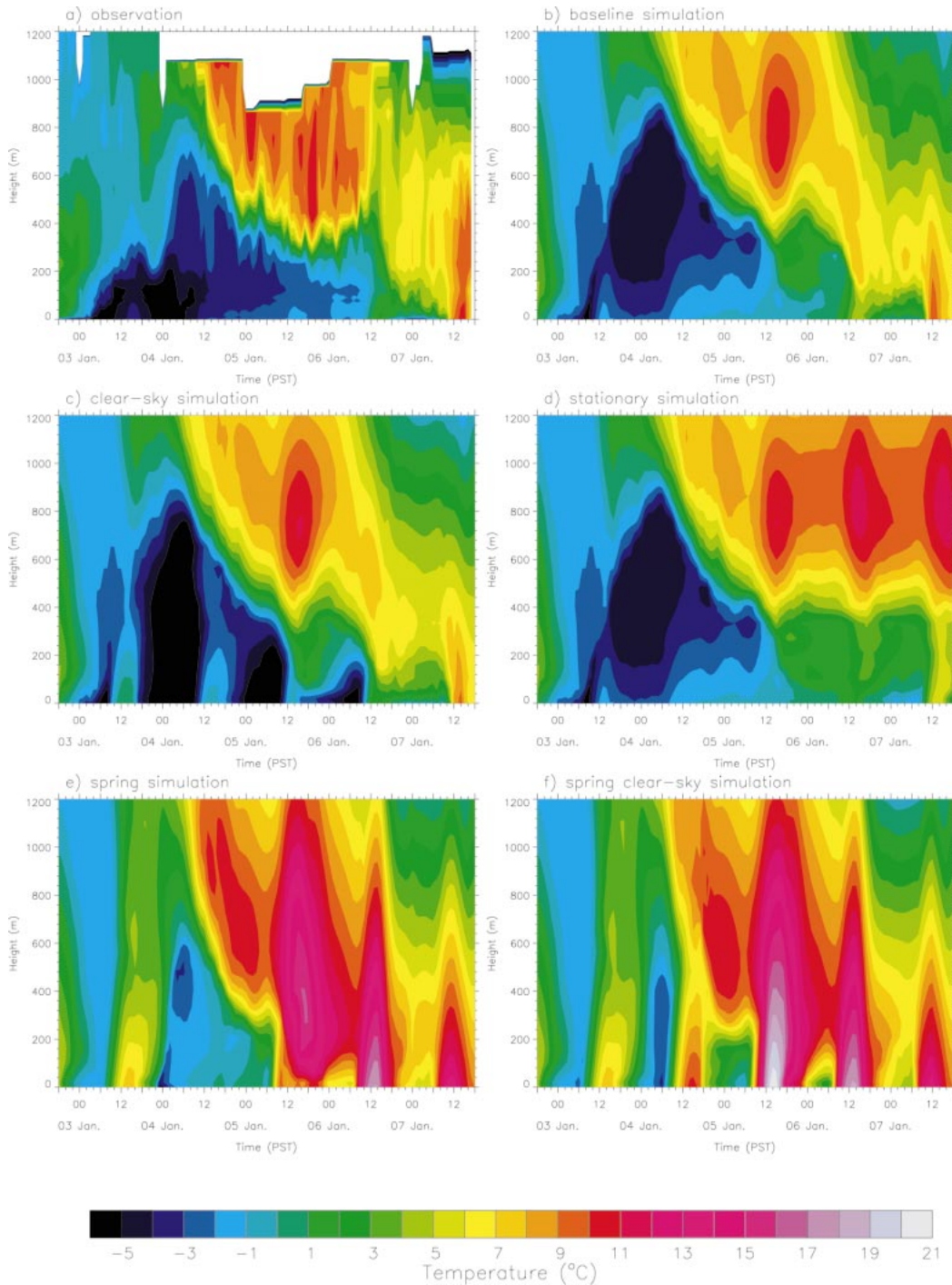


FIG. 3. Vertical temperature structure evolution at HMS during the period 1800 PST 2 Jan to 1800 PST 7 Jan from (a) the RASS and tower observations, (b) the baseline simulation, (c) the clear-sky simulation, (d) the stationary simulation, (e) the spring simulation, and (f) the spring clear-sky simulation.

northwesterly. On the afternoon of 6 January, the stratus dissipated, allowing solar radiation to penetrate to the surface and warm the lower atmosphere. But before the temperature inversion was completely destroyed, the sun set and a surface-based inversion layer formed by

longwave radiative cooling. Finally after sunrise on 7 January, solar heating on the basin floor destroyed the surface-based inversion, and a neutral to unstable boundary layer was established just after noon, marking the end of this cold pool episode.

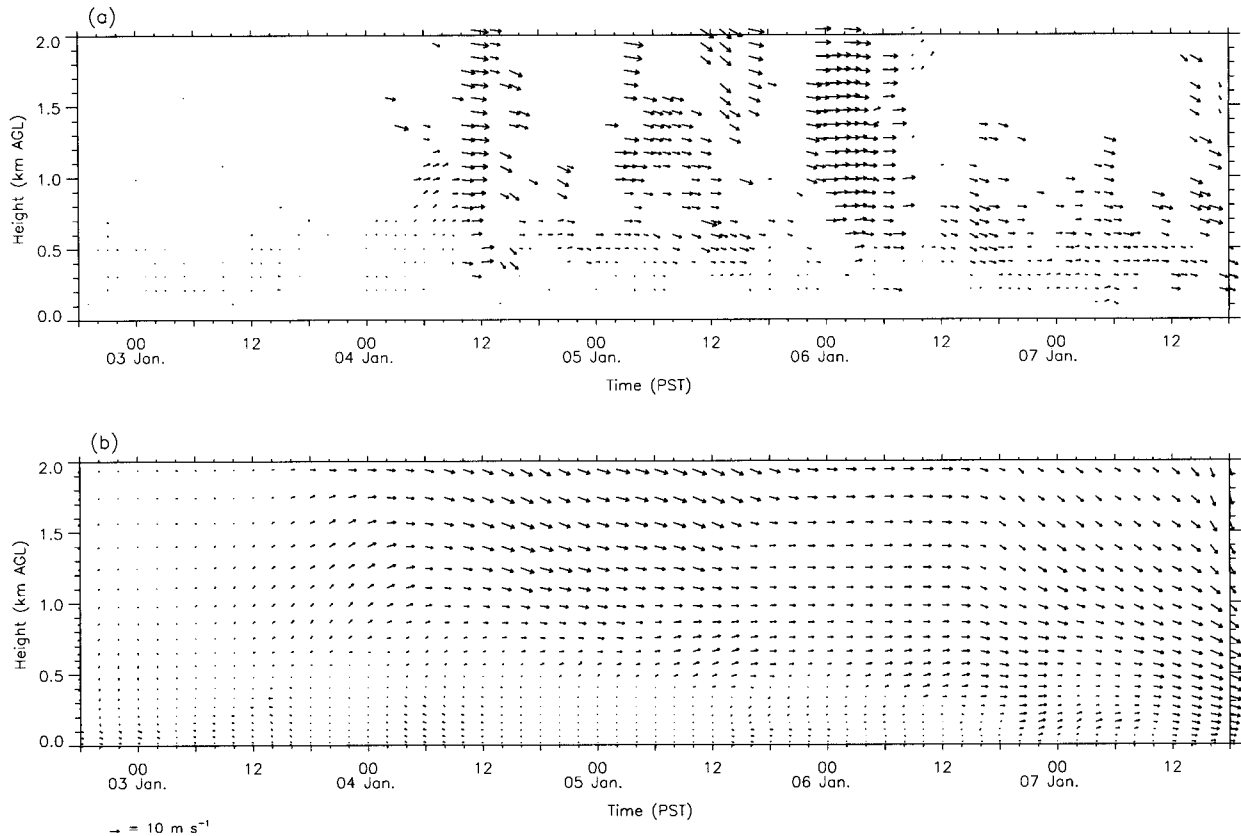


FIG. 4. Time–height distribution of horizontal wind vectors at HMS for the period from 1800 PST 2 Jan to 1800 PST 7 Jan from (a) radar wind profiler observations and (b) the baseline simulation.

Although limited by the rather poor data recovery rate due to low humidity and weak turbulence, the radar wind profiler measurements in Fig. 4a indicated weak winds inside the cold pool as the lower atmosphere was decoupled from layers aloft by the capping inversion. Above the cold pool, winds were moderate to strong most of the time except near the beginning of the episode when the region was under the control of a high pressure center. Wind directions aloft were mostly westerly during 4 and 5 January, shifting to northwesterly later on 6 and 7 January. Wind speeds inside the cold pool began to increase during the evening of 6 January. The increase first occurred in the upper portion of the pool as the inversion cap was removed, and finally at the surface when the surface-based nocturnal temperature inversion was destroyed.

It is useful to divide the evolution of this cold pool into four different stages. The first was an initialization stage during the night of 2 January and the morning of 3 January when cold air began to accumulate in the basin to form a temperature inversion. The second stage was the maintenance stage from the afternoon of 3 January through the early morning of 6 January during which low-level cloudiness prevented convective warming at the base of the cold pool and the strong capping

inversion confined the cold air within the basin. The third stage was the decay stage on 6 January when the inversion cap on top of the cold pool was weakened significantly by cold air advection aloft, and surface heating occurred in the afternoon as the low-level stratus deck dissipated. Finally, the breakup stage occurred on 7 January when the temperature inversion was completely destroyed as cold air advection occurred aloft and as an unstable boundary layer grew upward from the heated ground.

### 3. Model

It is clear from the above discussion that various mechanisms, including large-scale subsidence and temperature advection, mesoscale downslope warming, fog or cloud formation, and surface radiative heating or cooling, may have all played a role in the formation and destruction of this cold pool episode. The relative importance of these mechanisms at different stages of the cold pool evolution cycle, however, is not clear. To investigate the contributions of various mechanisms to the formation, maintenance, and destruction of this persistent cold pool, we conducted a series of numerical simulations using a mesoscale numerical model.

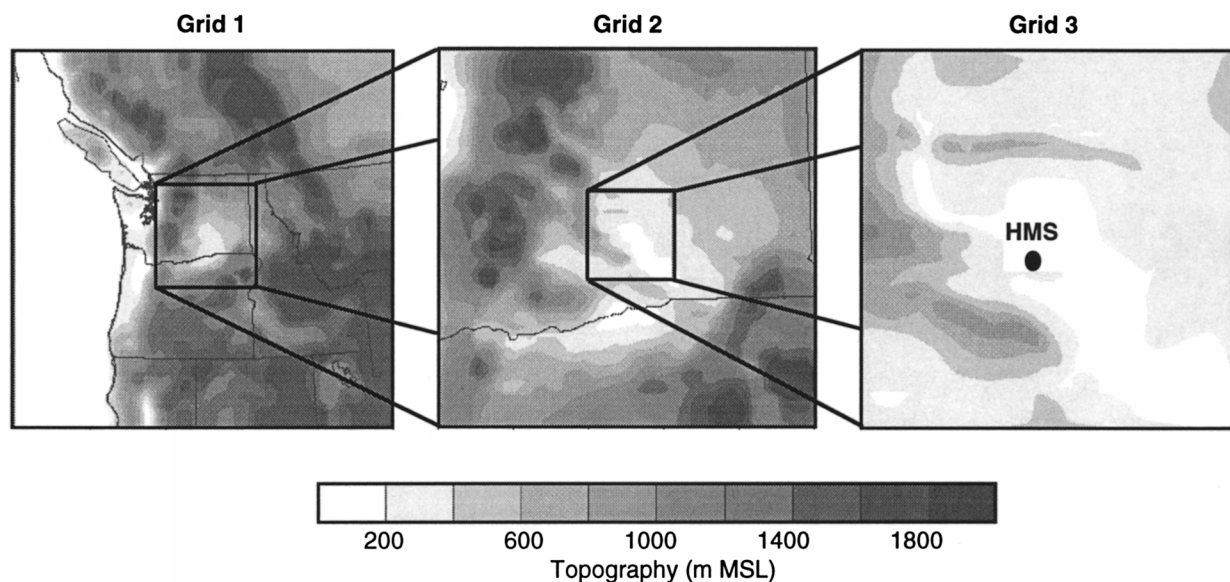


FIG. 5. Modeling domains and topography in each domain.

The model used for this study was the Regional Atmospheric Modeling System (RAMS), a three-dimensional, nonhydrostatic, mesoscale model. A detailed description of the RAMS model was given by Pielke et al. (1992). The optional physical parameterizations employed for the present application included the Mellor and Yamada (1982) level-2.5 turbulence parameterization scheme, the Louis (1979) boundary layer parameterization, and the Chen and Cotton (1983) radiation schemes that include the impact of clouds on both short- and longwave radiation. RAMS contains a full cloud microphysics scheme, but for this study the diagnostic cloud scheme in RAMS was used to reduce computational costs.

RAMS was configured with three nested two-way interactive grids as shown in Fig. 5. The outer grid, at a horizontal resolution of 32 km, extended from western Wyoming to the Pacific Ocean and from northern California to British Columbia. The middle grid, with a horizontal resolution of 8 km, encompassed the Columbia basin and the surrounding mountains. The inner grid, at 2-km resolution, included the Pasco subbasin with its center over HMS. RAMS employs a terrain-following, or sigma, coordinate system and, for this study, 42 sigma levels were used with 14 placed in the lowest 1000 m in all three grids to resolve the vertical structure of the cold pool, especially the shallow inversion cap at the top of the pool. Land use types for the three RAMS grids were specified based on a U.S. Geological Survey 1-km dataset for North America, and surface temperatures at the ocean grid points were determined by interpolation from 2-week-composite satellite-derived sea surface temperatures at 1° latitude–longitude horizontal resolution.

The National Centers for Environmental Prediction

Aviation Model (AVN) and Eta Model analyses were used to provide the initial and boundary conditions for the RAMS simulations. The RAMS simulations with the AVN Model analyses yielded slightly better overall results than those with the Eta Model analyses. This is generally consistent with the experience of weather forecasters in the Columbia basin (G. Reinecke and P. Perrault, HMS, 2000, personal communication; J. Mittelstadt, National Weather Service Forecast Office, Pendleton, OR, 2000, personal communication) who indicate that the AVN Model usually outperforms the Eta Model in forecasts for the Columbia basin. For this reason, we used the AVN Model analyses to provide the initial and boundary conditions for the RAMS simulations described below. All simulations were initiated at 0000 UTC 3 January (1600 PST 2 Jan) and ended at 0000 UTC 8 January (1600 PST 7 Jan) and the time steps used for the three grids were 40, 20, and 10 sec, respectively. Because the purpose of this model application was to study physical mechanisms, no data assimilation was used in the RAMS simulations except at the lateral boundaries of the outer grid where the model results were “nudged” toward the AVN model analyses.

#### 4. Mechanisms governing cold pool evolution

A series of numerical simulations were performed to investigate individual mechanisms important for the formation, maintenance, and removal of this persistent cold pool.

##### a. The baseline simulation

A baseline simulation was designed to capture the observed temperature and wind structure evolution dur-

ing the cold pool episode. A comparison of the baseline simulation with observations should allow us to determine the uncertainties in the simulation and provide a basis for explaining results from subsequent numerical simulations designed to isolate individual mechanisms. The full set of model physics and realistic initial and boundary conditions were used in the baseline simulation in order to achieve the best model performance.

The temperature structure evolution over HMS for the 5-day period from the baseline simulation is shown in Fig. 3b. A comparison of Fig. 3b with the observed temperature variations in Fig. 3a indicates that the model was able to capture the principal features of the observed changes in temperature structure during this cold pool episode. These include the initiation of the cold pool during the night of 2 January and the early morning of 3 January, the rapid warming of the air aloft on 4 and 5 January, the formation of a strong capping inversion layer and its descent with time, the decrease of the temperatures aloft on 6 January and the subsequent removal of the inversion cap, the development of the nocturnal inversion during the night of 6 January, and finally, the upward growth of an unstable boundary layer on 7 January.

Although the baseline simulation was able to capture the principal features at each stage of the cold pool evolution, it failed to reproduce some of the details of the evolving temperature structure. Differences between the simulated and observed temperature structure include 1) the simulated temperatures were somewhat colder during the initialization stage on 3 January, 2) the simulated temperature gradients in the capping inversion layer were not as sharp as observed, 3) the simulated surface-based inversion during the night on 6 January was deeper but weaker than observed, and 4) the simulated cold air advection during the decay and the breakup stages on 6 and 7 January penetrated somewhat deeper into the basin. In addition, differences also existed in the detailed vertical temperature distribution within the cold pool. For example, on 3 and 4 January, the coldest temperature in the simulation occurred in the mid-to-upper layers of the cold pool in the simulation instead of in the lower portion of the pool as observed. This could be attributed mainly, as we will show later, to the higher simulated base of low-level clouds during this time period, which, in turn, may be a result of the use of the simple diagnostic cloud scheme and/or limited vertical resolution.

The simulated winds over HMS are shown in Fig. 4b for every other hour during the 5-day period. The simulated winds are generally in good agreement with the available wind data. As in the wind profiler observations, the simulated winds are light and variable within the cold pool during most of the 5-day period until the last day when winds in the low levels strengthened considerably after the removal of the temperature inversion. Above the cold pool, the simulated winds are strong and westerly in the first half of the period, becoming

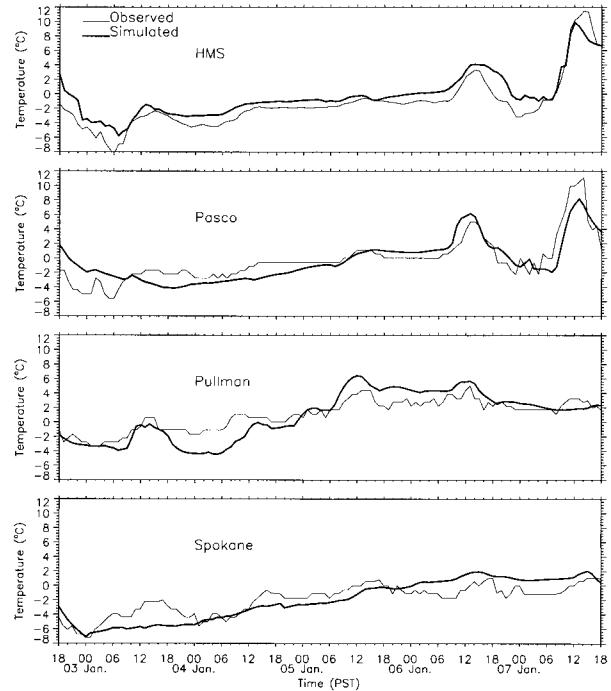


FIG. 6. Observed (thin line) and simulated (thick line) surface temperature evolution at several locations in eastern WA for the baseline simulation.

northwesterly in the second half, in agreement with the observed wind direction shift. The simulated wind speeds aloft, however, are somewhat lower than observed, and the simulated wind speed increases between 100 and 300 m AGL during the evening and the night of 6 January were not seen in the observations.

In addition to the comparisons between simulations and upper-air measurements, we also made comparisons (Fig. 6) between temperature simulations and temperature measurements made at selected surface weather stations operated by the National Weather Service in eastern Washington. The simulated temperatures were taken from the model grid points closest to the surface stations. Two of the four stations (HMS and Pasco) are within the RAMS inner grid (2-km grid spacing), while the other two (Spokane and Pullman) fall outside the inner grid but within the middle grid (8-km grid spacing.) Although there were some differences between the simulated and observed temperatures, the temperature variations at each individual station and the different patterns between the stations during this 5-day period were simulated reasonably well. It is interesting to note the differences in the observed temperature variations among the four stations. HMS (213 m MSL) and Pasco (116 m MSL), both located in the Pasco subbasin, showed increases of several degrees Celsius during the daytime on 6 January after a relatively steady 3-day period with below-freezing temperatures. The temperature dropped back to below freezing again during the night on 6 January. Larger increases occurred after sun-

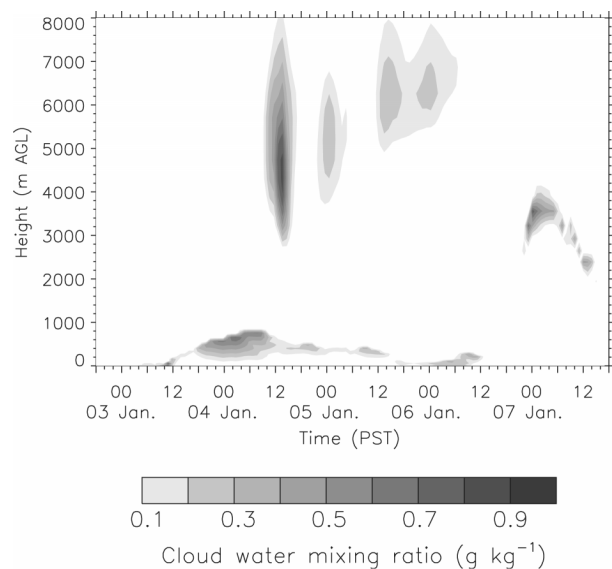


FIG. 7. Time–height cross section of cloud water mixing ratio at the grid point closest to HMS for the baseline simulation.

rise on 7 January, with the maximum temperature reaching over  $10^{\circ}\text{C}$  at noon. The surface temperature behavior at the two higher elevation stations located on the periphery of the Columbia basin was quite different. The temperature at Spokane (735 m MSL) remained below freezing throughout the time period, while at Pullman (773 m MSL) it was below freezing on 3 and 4 January, increased to about  $3^{\circ}\text{C}$  on the afternoons of 5 and 6 January, but only to slightly above  $1^{\circ}\text{C}$  on the afternoon of 7 January. The generally lower temperatures at Spokane and Pullman compared to those at HMS and Pasco were mainly a result of the increase in altitude from the basin floor to the basin rim.

#### b. Low-level cloudiness

Hourly surface observations made by forecasters at HMS (staffed 24 h on weekdays and 8 h on weekends) show that the 2–7 January cold pool episode was accompanied by a stratus overcast during most of the period. The nocturnal cooling during the clear night on 2 January produced fog on the morning of 3 January, which later lifted to form a stratus deck with cloud base varying between 60 and just over 300 m AGL. The low-level cloudiness remained over the basin for the next three days. The stratus cleared on the morning of 6 January, exposing the area to an overcast of altocumulus. The formation and dissipation of the low-level cloudiness were simulated reasonably well by the model. The simulated cloud water mixing ratio over HMS (Fig. 7) shows the presence of fog and low-level clouds from the early morning of 3 January until noon on 6 January except for a brief clearing around 1400 PST on 5 January. The simulated cloud bases, however, were somewhat higher than the observed bases and the final

clearing of fog and stratus on 6 January occurred 2 h later in the simulation.

Low-level clouds appear to be the main reason for the lack of diurnal temperature oscillation inside the cold pool, but it was unclear just how critical they were in maintaining the cold pool by blocking solar radiation and, therefore, reducing surface radiative heating. To answer this question, a second numerical simulation, called the clear-sky simulation, was performed in which clouds were not allowed to form even when the atmosphere was supersaturated. The predicted time–height cross section of temperature from the grid point nearest to HMS is shown for this simulation in Fig. 3c. Major differences between this and the baseline simulation (Fig. 3b) appear mainly in the lower portion of the cold pool. In the baseline simulation the presence of the low-level clouds helped to keep the temperature relatively steady, whereas the lack of clouds in the clear-sky simulation allowed solar radiation to penetrate to the surface during the day and more longwave radiation to escape from the atmosphere at night, producing diurnal temperature oscillations inside the cold pool. Compared to the temperatures from the baseline simulation, the daytime temperatures from the clear-sky simulation were higher and the nighttime temperatures were much lower. Despite the differences in the lower part of the cold pool, the simulated temperature structure and evolution during the course of the 5-day period and the time of the final breakup of the cold pool were surprisingly similar between the two simulations. This suggests that even in the absence of low-level cloudiness, the amount of solar heating on midwinter days was apparently insufficient to completely remove the deep cold air that accumulated in the basin and the strong capping inversion at the top of the cold pool. In other words, once a cold pool with a strong capping inversion is well established, the low-level cloudiness, when present, reduces diurnal temperature changes within the cold pool. The presence of low-level clouds, however, does not seem to be critical to the maintenance of the cold pool.

#### c. Downslope warming and temperature advection aloft

The north–south-oriented Cascade Mountains that form the western boundary of the Columbia basin rise to over 2500 m MSL. As strong westerly winds cross over the Cascade Mountains, the air that descends the lee slope experiences adiabatic warming, bringing warm air to the east side of the Cascades. This downslope warming is evident in Fig. 8, which shows contours of potential temperature along an east–west vertical cross section through HMS from the RAMS middle grid on 4 and 5 January. Since the period was primarily cloud free above the cold pool, it is safe to assume that any potential temperature changes were due to advection, not to diabatic processes. Although the values of po-

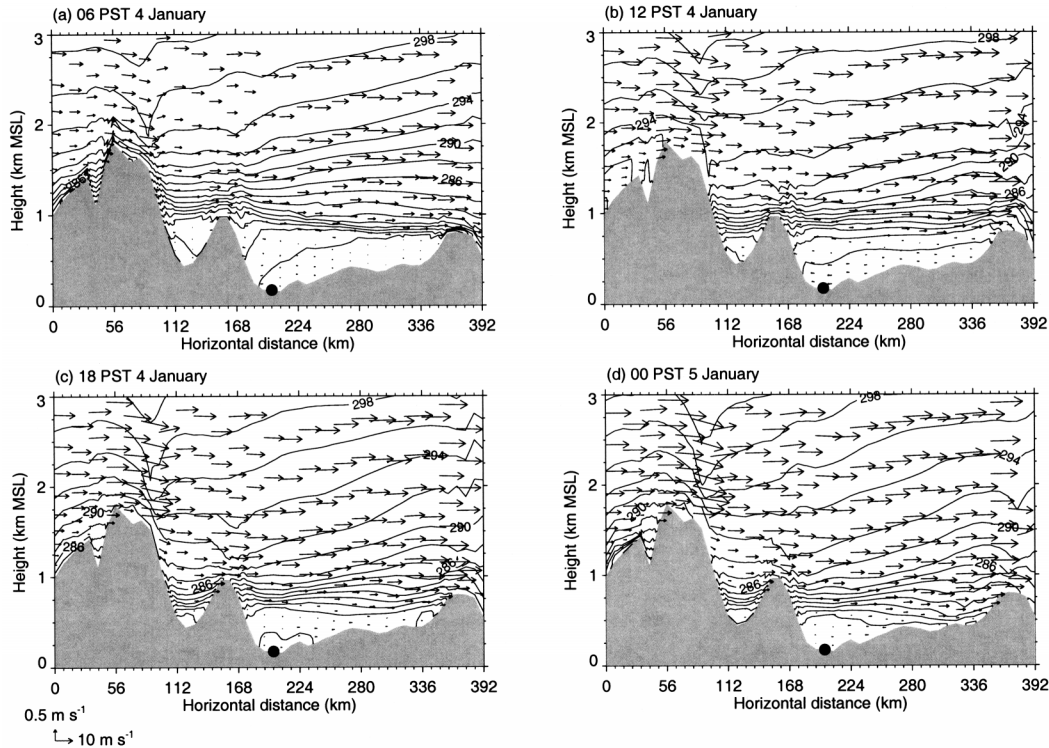


FIG. 8. Contours of potential temperatures on an east–west vertical cross section through HMS from the RAMS middle grid at four times in the baseline simulation beginning at 0600 PST 4 Jan and ending at 0000 PST 5 Jan. The black dot denotes the location of HMS on the cross section.

tential temperature did not change much during the period, the contours dropped in elevation as westerly flow across the Cascades intensified with time, indicating the effect of downward vertical advection. This downward vertical advection contributed to the warming of the layer above the cold pool and the descent of the inversion cap with time.

The role of the downslope warming in the formation of the strong capping inversion on top of the cold pool was further confirmed by an examination of the relative contributions to the local time rate of change of potential temperature from various terms in the thermodynamic equation. Figure 9 shows a time series of the four terms on the right-hand side of the thermodynamic equation and the resulting change of potential temperature as averaged horizontally over the area of the basin floor and vertically from approximately 400 to 800 m AGL. The four terms are (i) turbulent diffusion, (ii) horizontal advection, (iii) vertical advection, and (iv) radiative heating or cooling. It shows that the large rate of increase in potential temperature on 4 January was clearly caused by vertical instead of horizontal advection. The horizontal advection term was generally negative throughout the time period, which should lead to cooling rather than warming. Turbulence and radiative heating and cooling terms were negligibly small except for a brief period at the beginning of 4 January when the relatively large radiative cooling at cloud top occurred.

As suggested earlier, even in the absence of low-level clouds, daytime solar heating at the ground was not strong enough to break up the capping inversion that helped to keep cold air within the basin. It appeared that cold air advection associated with changes in synoptic ridge position was instrumental in destroying the strong inversion cap, which facilitated the removal of the cold air and terminated the persistent wintertime cold pool. To confirm this, a third model run, called the stationary simulation, was carried out in which the large-scale forcing, which affects the simulation results through the model boundaries, was kept unchanged after 0000 UTC on 6 January (1600 PST on 5 Jan). Since cold advection aloft did not begin until the morning of 6 January, this eliminated the possible influence of large-scale cold air advection aloft on the model results. The simulated temperature evolution at HMS from the stationary simulation is shown in Fig. 3d. The capping inversion from this simulation persisted until the end of the period and there was no sign of the cold pool breakup that occurred on 7 January in the baseline simulation. Temperatures increased considerably on the morning of 7 January in the absence of a low-level cloud deck, but the temperature increases resulted only in an isothermal atmosphere, which is still thermodynamically stable. These results confirm that cold air advection aloft associated with changes in synoptic pressure patterns was

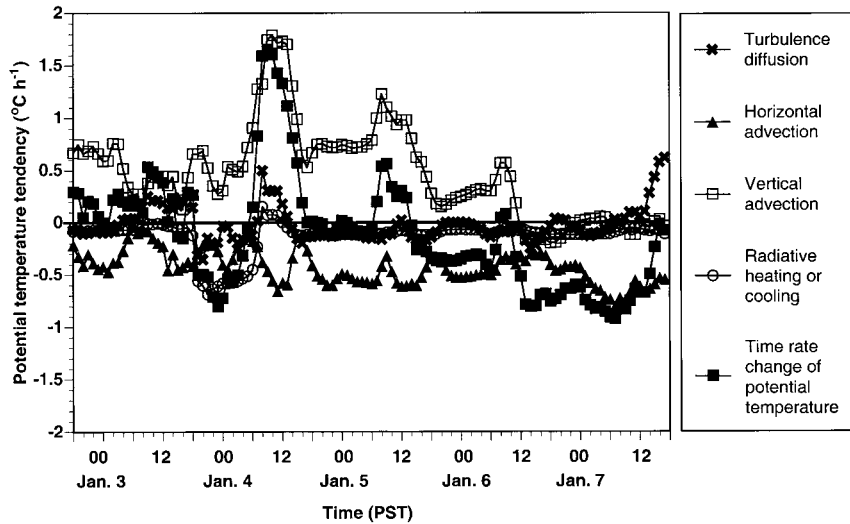


FIG. 9. Hourly values of the terms in the thermodynamic equation from the baseline simulation as averaged horizontally over the area of the basin floor and vertically from approximately 400 to 800 m MSL.

largely responsible for the removal of the strong capping inversion and the termination of this cold pool episode.

*d. Surface radiative heating and cooling*

The previous discussions have shown that this persistent wintertime cold pool with capping inversion, once well established, is unlikely to be destroyed solely by the weak wintertime insolation even in the absence of low-level cloudiness. Climatological analyses performed by Whiteman et al. (2001) indicate that persistent cold air pools occur predominantly in the two winter months of December and January in the Pasco subbasin.

Cold pools observed in late fall or early spring tend to be nonpersistent or diurnal cold pools that form during the evening or night and decay following sunrise the next day. The role of the seasonal change of insolation on cold pool evolution was investigated by running another set of numerical simulations (spring and spring clear-sky) to determine whether daytime solar heating of the ground in early spring is able to break the inversion and result in a diurnal cold pool instead of a persistent one. The two simulations essentially repeated the baseline and clear-sky simulations except that a starting date of 10 March instead of 2 January was used for radiative flux calculations.

The changes of temperature with time and altitude over HMS from the two simulations are shown in Figs. 3e and 3f. The patterns on the two figures were similar on the first and the last two days when a convective boundary layer developed in the afternoon followed by a stable boundary layer at night. The differences on these days are small, with the temperatures for the spring clear-sky simulation slightly lower at night and higher during the day than for the spring simulation. Significant differences, however, existed during the middle two days when low-level clouds were present in one (spring) but not in the other (spring clear-sky) simulation, as shown by the cloud water mixing ratio in Fig. 10. In the absence of low-level cloudiness, the daytime solar heating in early spring apparently was sufficient to break the capping inversion and allow the cold air accumulated in the basin during the night to be completely removed in the daytime. When low-level clouds were present, sunlight could not penetrate to the basin floor and the inversion could persist through the next day. Thus, the absence or presence of low-level clouds during

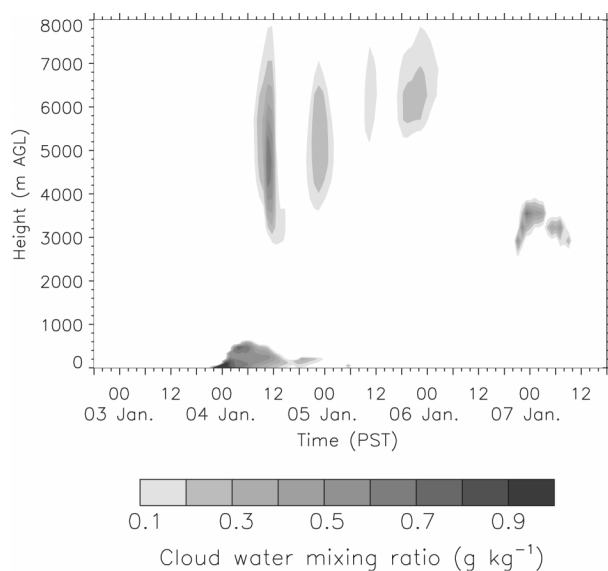


FIG. 10. Same as in Fig. 7 but for the spring simulation.

a cold pool in spring may determine the type of cold pool to be either a diurnal cold pool or a persistent one.

A comparison of the temperature variation from the spring simulation in Fig. 3e with that from the baseline simulation in Fig. 3b revealed that for the same synoptic forcing the differences in radiative fluxes between mid-winter and early spring can make a significant difference in cold pool evolution. The cold pool episode began in the baseline simulation on the first evening and lasted till the morning of the last day. In the spring simulation, however, the cold pool started a day later on the second evening following the collapse of an afternoon convective boundary layer, and the temperature inversion was broken a day earlier.

#### e. Turbulent erosion

One of the principal features of a cold pool is that winds are normally light and variable within the pool, regardless of whether winds aloft are weak or strong. When winds aloft are strong, large vertical wind shears can occur across the top of the pool. Turbulence generated by the strong wind shear may erode the temperature inversion layer by layer beginning at the top of the pool. This “turbulent erosion” has been proposed as a potential mechanism for cold pool destruction. Vrhovec and Hrabar (1996) studied turbulent erosion at the top of a cold pool in a small idealized basin cross section using a 2D numerical model. For a 200-m-deep cold pool capped by a 50-m-thick inversion layer with a 3-K temperature difference, their simulation showed that dissipation of the inversion began to occur when wind speed at the top of the pool reached  $15 \text{ m s}^{-1}$ , and it could take up to 11 h for the turbulent erosion to completely dissipate the cold pool. They noted that since this timescale is longer than the period of daylight during the cold half of the year, it is possible for radiative cooling to start to produce a new nocturnal inversion before the old one is completely dissipated. Because of the difficulty of measuring turbulence aloft, no data are yet available to support these model results regarding turbulent erosion of a cold pool.

In the case of the cold pool studied here, large vertical wind shears occurred near the top of the pool during most of the 5-day period, except on the first day when winds aloft were also weak, and near the end when strong winds penetrated down to the surface. To determine whether turbulent erosion played a role in the dissipation of this cold pool, especially in the descent of the inversion cap from 700–800 m to below 500 m during 4 and 5 January, we examined the turbulent kinetic energy (TKE) fields predicted by the model from the baseline simulation. Figure 11 shows a time–height cross section of TKE over HMS with the approximate base of the capping inversion, or the top of the cold pool, indicated by the  $0^\circ\text{C}$  temperature contour. Surprisingly, no TKE was generated near the top of the cold pool despite the large wind shear there. Instead,

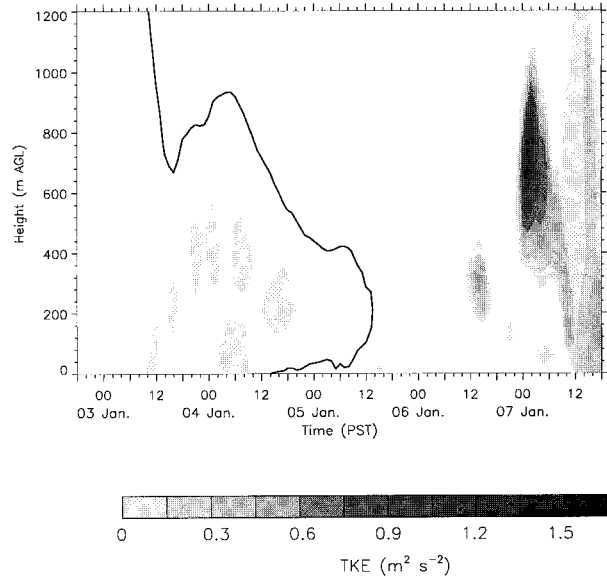


FIG. 11. Time–height cross section of TKE over HMS for the baseline simulation. The thick line is the  $0^\circ\text{C}$  temperature contour, which indicates the approximate base of the capping inversion.

TKE was produced *within* the cold pool, although the TKE values were generally small. This TKE production inside the cold pool was a result of radiative cooling near the cloud top and the subsequent downward convection. Large TKE values were produced near the end of the cold pool episode when the stratification changed from very stable to near neutral/unstable in the lower atmosphere. The TKE contours on an east–west cross section through HMS in Fig. 12 also show little TKE production associated with wind shear near the top of the cold pool. Large TKE values were found over the ridgetops.

The reason that little turbulent mixing was generated near the cold pool top is revealed in Fig. 13, which shows the shear and buoyancy production rates and the resulting TKE production rate over HMS at 1200 PST 5 January. The shear production rate was determined from

$$P_s = K_m \left[ \left( \frac{\partial u}{\partial z} \right)^2 + \left( \frac{\partial v}{\partial z} \right)^2 \right],$$

and the buoyancy production was calculated by

$$P_b = -K_h \frac{g}{\theta} \frac{\partial \theta}{\partial z},$$

where  $K_m$  and  $K_h$  are eddy diffusivities for momentum and heat, which are functions of the mixing length scale and TKE.

In the lower and middle part of the cold pool, shear production was small because winds were nearly calm with very little wind shear. The small shear production was overwhelmed by the negative buoyancy production that was large within the cold pool except in the lowest

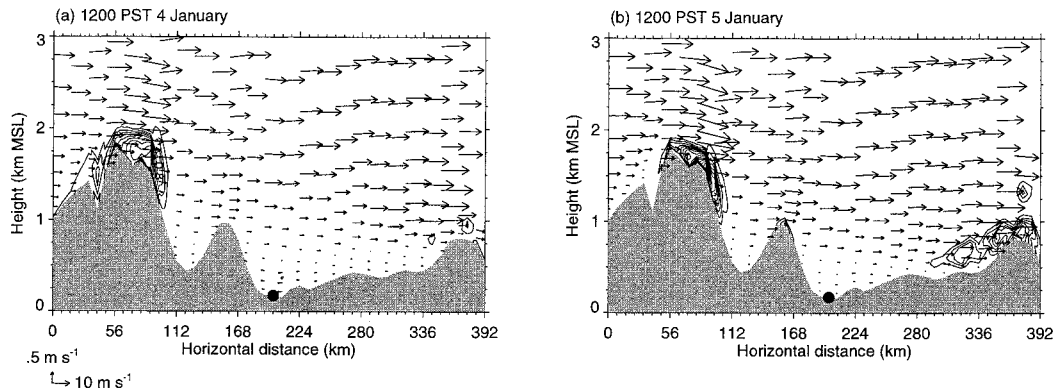


FIG. 12. Turbulent kinetic energy on an east–west cross section through HMS at 1200 PST on (a) 4 Jan and (b) 5 Jan for the baseline simulation. The black dot denotes the location of HMS on the cross section.

200 m where the stratification was near neutral as a result of cloud cover. Near the top of the cold pool, shear production increased considerably as wind speeds changed from near calm beneath the top to moderate/strong above it. The negative buoyancy production, however, also increased significantly in the same layer with a strong temperature inversion across the top of the pool, which counterbalanced the positive shear production and resulted in a negative net TKE production rate.

Notice that the combination of only moderate wind shear and a strong inversion cap made this cold pool case not particularly favorable for turbulence production near the top of the cold pool. Other cold pools that have either a weaker temperature jump at the top or stronger wind shears may allow turbulence to be generated near the top and turbulent erosion to occur. For example, diurnal cold pools often have much weaker stability at

the top than persistent cold pools and, therefore, are more likely to be affected by shear-generated turbulence and erosion at the cold pool top.

## 5. Conclusions

Cold pools are a prominent wintertime meteorological phenomenon in many basins of the world. Cold pool evolution is affected by atmospheric processes that occur on multiple scales, for example, synoptic-scale subsidence and temperature advection, mesoscale downslope warming, cold or warm frontal passages, local radiative heating and cooling at the surface, cloud formation with associated latent heat release and radiative cooling at cloud top, turbulent erosion, and convective boundary layer development. In this paper, we have used a set of numerical simulations to investigate the role of several of these processes in the evolution of a multiday wintertime cold pool that occurred in the Columbia basin in January 1999.

The simulations indicated that the formation of this multiday cold pool was a result of cold air being trapped by a strong capping inversion that was produced primarily by downslope warming as strong westerly winds descended in the lee of the Cascades Mountains. The breakup of the strong inversion cap was caused by large-scale cold air advection aloft, which, together with surface heating and turbulent mixing, led to the destruction of the cold pool. The fog or stratus deck, a feature frequently associated with wintertime cold pools, reduced diurnal oscillations of temperatures within the pool by keeping direct sunlight from penetrating to the basin floor. The presence of low-level clouds, however, was not critical to the maintenance of this wintertime cold pool because surface solar heating on a midwinter day is insufficient, even in the absence of low-level cloudiness, to break the persistent temperature inversion. In the spring when insolation is much stronger, the presence of low-level clouds becomes much more important for the development of a multiday cold pool. Turbulent erosion, a potential mechanism for removing

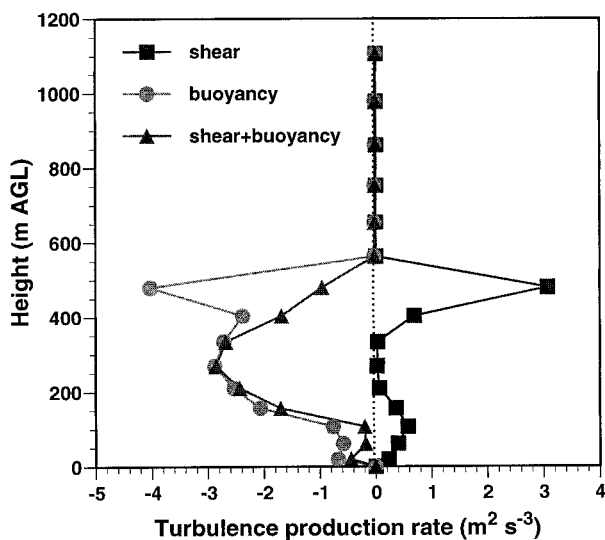


FIG. 13. Vertical profiles of the turbulent kinetic energy production rate by wind shear and buoyancy over HMS at 1200 PST 5 Jan for the baseline simulation.

cold air from the top of the pool, was found to be insignificant for this cold pool case because the positive turbulence production due to vertical wind shear between the quiescent air within the pool and the stronger winds aloft was counterbalanced by the negative buoyancy associated with the strong temperature inversion cap near the top of the pool.

It is worth pointing out that this is a model-based study and that the above conclusions came largely from the RAMS model simulations. While the model appears to have captured the main features of this cold pool event, it did not produce all the details of the observed temperature structure and evolution. One of the major limitations is the uncertainty associated with the prescribed soil moisture values, which has a major impact on the near-surface moisture and temperature evolution as well as the formation of fog and low-level stratiform clouds. A better knowledge of the soil moisture and its spatial distribution should improve the simulation. Better model resolution, especially in the vertical direction, should also result in a more detailed description of the cold pool evolution. The fact that the model failed to capture all the details in the observations, however, should not affect the conclusions drawn regarding the role of various physical processes in the formation, maintenance, and destruction of this persistent wintertime cold pool. It is expected that other nested grid mesoscale models would perform similarly in simulating such cold pool events as long as they have adequate treatment of multiscale forcing, such as synoptic-scale subsidence and advection, mesoscale downslope flows, local formation of fog and low-level stratiform clouds, and cloud and radiation interaction.

*Acknowledgments.* We would like to thank Dr. Jon Mittelstadt at the National Weather Service Forecast Office in Pendleton, Oregon, for useful discussions. The paper benefited from review comments provided by John Walsh and two anonymous reviewers. This re-

search was supported by the U.S. Department of Energy under Contract DE-AC06-76RL0 1830 at the Pacific Northwest National Laboratory under the auspices of the Environmental Meteorology Program. Pacific Northwest National Laboratory is operated for the U.S. Department of Energy by Battelle Memorial Institute.

#### REFERENCES

- Chen, S., and W. R. Cotton, 1983: A one-dimensional simulation of a stratocumulus-capped mixed layer. *Bound.-Layer Meteor.*, **25**, 289–321.
- Lee, T. J., R. A. Pielke, R. C. Kessler, and J. Weaver, 1989: Influence of cold pools downstream of mountain barriers on downslope winds and flushing. *Mon. Wea. Rev.*, **117**, 2041–2058.
- Louis, J. F., 1979: A parametric model of vertical eddy fluxes in the atmosphere. *Bound.-Layer Meteor.*, **17**, 187–202.
- Mayr, G. J., and T. B. McKee, 1995: Observations of the evolution of orogenic blocking. *Mon. Wea. Rev.*, **123**, 1447–1464.
- Mellor, G. L., and T. Yamada, 1982: Development of a turbulent closure model for geophysical fluid problems. *Rev. Geophys.*, **20**, 851–875.
- Petkovsek, Z., 1992: Turbulent dissipation of cold air lake in a basin. *Meteor. Atmos. Phys.*, **47**, 237–245.
- Pielke, R. A., and Coauthors, 1992: A comprehensive meteorological modeling system—RAMS. *Meteor. Atmos. Phys.*, **49**, 69–91.
- Savoie, M. H., and T. B. McKee, 1995: The role of wintertime radiation in maintaining and destroying stable layers. *Theor. Appl. Climatol.*, **52**, 43–54.
- Smith, R., and Coauthors, 1997: Local and remote effects of mountains on weather: Research needs and opportunities. *Bull. Amer. Meteor. Soc.*, **78**, 877–892.
- Vrhovec, T., 1991: A cold air lake formation in a basin—A simulation with a mesoscale numerical model. *Meteor. Atmos. Phys.*, **46**, 91–99.
- , and A. Hrabar, 1996: Numerical simulations of dissipation of dry temperature inversions in basins. *Geofizika*, **13**, 81–96.
- Whiteman, C. D., X. Bian, and S. Zhong, 1999: Wintertime evolution of the temperature inversion in the Colorado Plateau Basin. *J. Appl. Meteor.*, **38**, 1103–1117.
- , S. Zhong, W. J. Shaw, J. M. Hubbe, X. Bian, and J. Mittelstadt, 2001: Cold pools in the Columbia Basin. *Wea. Forecasting*, **16**, 432–447.
- Wolyn, P. G., and T. B. McKee, 1989: Deep stable layers in the intermountain western United States. *Mon. Wea. Rev.*, **117**, 461–472.